

# Onboard Radar Processing Development for Rapid Response Applications

Yunling Lou, Steve Chien, Duane Clark, Josh Doubleday, Ron Muellerschoen, and Charles C. Wang  
Jet Propulsion Laboratory, California Institute of Technology  
4800 Oak Grove Drive, Pasadena, CA  
Correspondence author: Yunling.Lou@jpl.nasa.gov

**Abstract - We are developing onboard processor (OBP) technology to streamline data acquisition on-demand and explore the potential of the L-band SAR instrument onboard the proposed DESDynI mission and UAVSAR for rapid response applications. The technology would enable the observation and use of surface change data over rapidly evolving natural hazards, both as an aid to scientific understanding and to provide timely data to agencies responsible for the management and mitigation of natural disasters. We are adapting complex science algorithms for surface water extent to detect flooding, snow/water/ice classification to assist in transportation/shipping forecasts, and repeat-pass change detection to detect disturbances. We are near completion of the development of a custom FPGA board to meet the specific memory and processing needs of L-band SAR processor algorithms and high speed interfaces to reformat and route raw radar data to/from the FPGA processor board. We have also developed a high fidelity Matlab model of the SAR processor that is modularized and parameterized for ease to prototype various SAR processor algorithms targeted for the FPGA. We will be testing the OBP and rapid response algorithms with UAVSAR data to determine the fidelity of the products.**

## I. INTRODUCTION

The DESDynI mission utilizes repeat-pass interferometric synthetic aperture radar (InSAR) to study deformation, ecosystem system structure, and the dynamics of ice. The L-band polarimetric SAR instrument is expected to operate at high data rate (1 -2 Gbps instantaneous or ~ 350 Mbps orbital average) to meet the high resolution and extensive coverage of the proposed measurements. Appropriate onboard processing technology could reduce onboard data storage and downlink data volume for some non-interferometric data products and expand the utility of the mission by providing rapid response capability. By reducing the downlink data rate from 400 Mbps to less than 1Mbps will enable us to downlink data more frequently by utilizing the S-band transponders available at many ground receiving stations. By generating selected data products onboard the spacecraft such as change detection and classification maps will enable us to

provide rapid response to needed measurements over rapidly evolving natural hazards such as flooding and volcanic eruptions.

We have been developing an onboard processor (OBP) concept for rapid response in our NASA funded Advanced Information System Technology task. This OBP concept consists of four major functions:

1. Control processor – ingest ephemeris data, generate processor parameters, retrieve reference data set if needed for repeat-pass product generation such as change detection.
2. SAR image formation – form single look compressed (SLC) image and interferogram with reference SLC image if requested.
3. Image compression – compress interferogram or polarimetric data with traditional image compression algorithms.
4. Product generation – generate geophysical products such as forest biomass, flood scene map, sea ice classification, and change detection.

Figure 1 shows the OBP scenario for rapid response applications for UAVSAR, the airborne repeat-pass interferometric synthetic aperture radar testbed [1]. We can reduce the downlink volume by a factor of 1000 or more, which will allow us to downlink the results via a satellite phone modem at the rate of ~ 100kbps. Using the satellite phone downlink will make targeted, critical information readily available to disaster response agencies in a timely manner.

The processor architecture, as shown in Figure 2, is based on the OBP developed for UAVSAR. We chose a hybrid architecture where we use a general-purpose microprocessor for data-dependent calculations that are performed occasionally and all other arithmetic operations that operate on every radar pulse in the field programmable gate array (FPGA). We demonstrated real-time SAR image formation with the custom FPGA processor board. Two FPGA processor boards are built to process data from two polarization channels or two interferometric channels at the

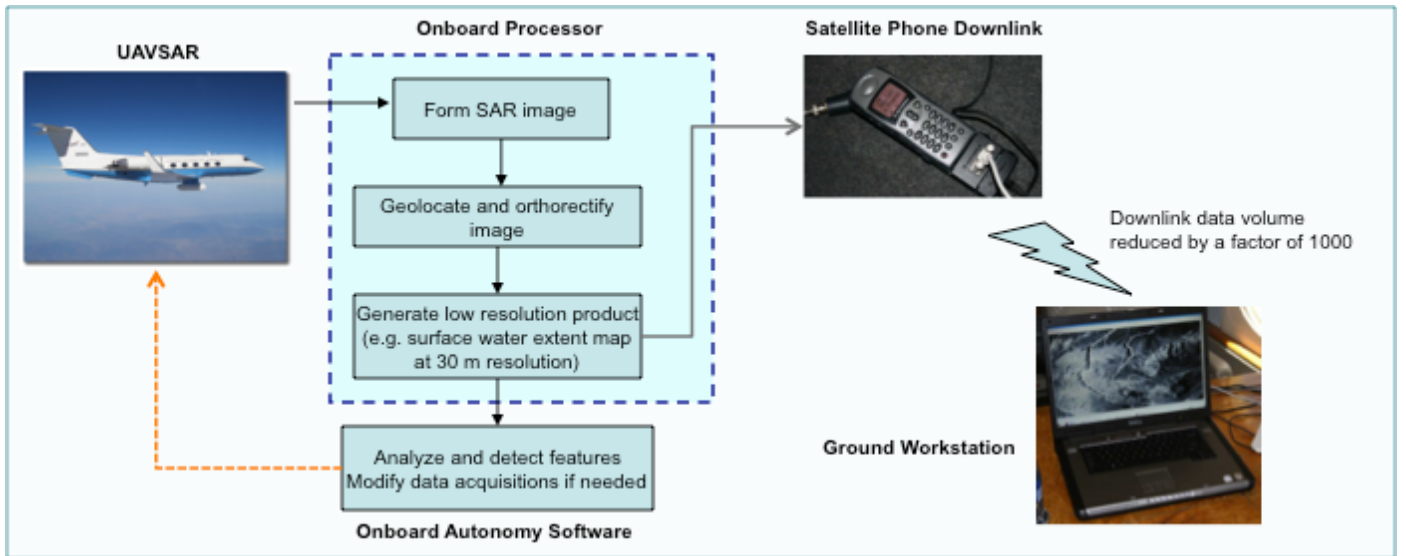


Fig. 1. OBP scenario for UAVSAR’s L-band polarimetric repeat-pass InSAR instrument.

same time. The availability of dual-polarized data and repeat-pass interferometric data enable us to generate quick-look science products based on unsupervised classification of polarimetric data and change detection respectively. In this paper, we present example data products that can be generated onboard the spacecraft for rapid response applications.

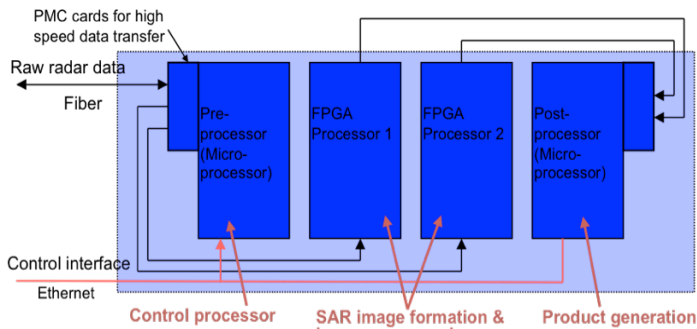


Fig. 2. UAVSAR OBP hardware architecture, where general purpose microprocessors are used for control processing and product generation and custom FPGA processor boards are used for SAR image formation and image compression.

## II. FPGA PROCESSOR DEVELOPMENT

### A. OBP Hardware Development

We developed a custom FPGA processor board in cPCI form factor that meets our specific needs, which included:

- Several fast random access memories (RAMs) for use as lookup tables and small working buffers
- Large double data rate (DDR) buffer for SAR processing
- Two Virtex-5 FPGAs for additional computing power
- Ability to load FPGA firmware via the PCI bus

We also completed development of a PMC interface board, which has a fiber-channel to RocketIO interface for receiving and reformatting high rate data from the radar and streaming

them into the FPGA processor board. We have implemented the FPGA code necessary to interface with the control register, the 2.5 Gbps serializer/deserializer (SERDES) links, and various memory banks. We are in the process of porting the SAR processing code to the FPGA for UAVSAR real-time SAR image formation demonstration.

### B. OBP SAR Processing Algorithm Development

We are developing an onboard processor model for studying the performance of radar processing algorithms when implemented in the OBP. Previously we used a “bit-close” model for modeling the processor functions and hardware operations. We subsequently realized that in order to have the fidelity to model high precision processor with stringent gain and phase requirements, a “bit-true” model is necessary to replicate exactly the hardware operations. For example, in hardware, we may use a Taylor series expansion to compute the square root of a number. In the “bit-true” model, we replicate the Taylor expansion instead of calling the square root function in Matlab. Portions of this OBP model will be used for future spaceborne radar developments, including DESDynI, SWOT, and the Europa sounder.

The Matlab OBP model is modularized and parameterized for ease to explore different processor implementations. This model has been verified against a “golden model” to determine performance. To improve simulation speed, we replaced many of the Matlab built-in fixed-point object and library with our own custom, fast, fixed-point object. We have developed libraries for fixed-point complex numbers, arithmetic operations (+, -, x, /, etc.), relational operators (<, >, ==, etc.), trigonometry, and re-quantization. We also developed techniques for measuring the statistics of floating-point operations, which are used to design fixed-point bit widths.

### III. RAPID RESPONSE APPLICATIONS

#### A. Surface Water Mapping and Flood Detection

We have generated a Surface Water Extent product that is potentially useful for flood disaster mitigation and less direct applications, such as in disease vector management. Our algorithm is based on estimating the dielectric constant of the observed area from polarimetric backscatter images, using an empirical formula as seen in work published by Dubios et. al. in 1995 [2], also based on L-band Polarimetric data, similar to the proposed DESDynI instrument and UAVSAR. With an image of the dielectric constant, we threshold for values exceeding 15 and classify these as water. Limitations on the empirical formula require filtering out pixels of significant vegetation, which we estimate with a Radar Vegetation Index (RVI), as well as areas of atypical local-incidence angle (<30 degrees) as computed from the flight telemetry and a digital elevation model.

Figure 3 is an example of this product, covering a portion of the Florida Everglades area. We chose this area as a proxy for floodwater as we have a substantial amount of data covering this region with a good balance of surface area of land versus water. Theoretically there should be no difference in detection between deep water and shallower floodwater. However, Figure 3 illustrates one of the potential pitfalls of this approach – surface roughness of the water can lead to false negatives (water being classified as land). Characterizing the surface conditions leading to this false classification, and whether this condition would be problematic in inland flooding scenarios (as opposed to open-waters) is work left for the future.

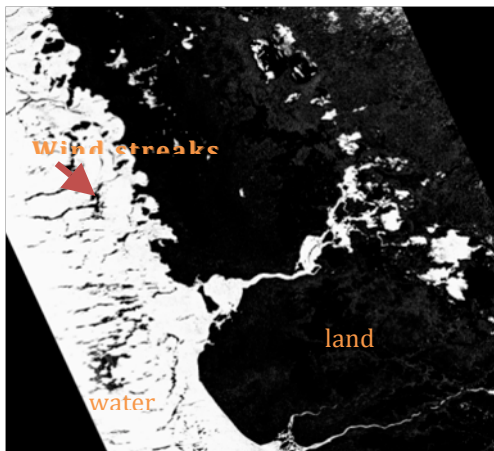


Fig. 3. Surface water extent map of Florida Everglades. White: water, black: non-water. Dark streaks on left are false negatives (assumed from surface roughening from wind).

#### B. Snow/Ice/Water Classification

Polarimetric SAR data have been used for sea ice detection and classification since this was first demonstrated with SIR-C data acquired in 1994 [3]. HV-intensity and HH/VV ratio and

anisotropy have been used for sea ice edge/open water detection. In this study we used a support vector machine approach to classify UAVSAR observation images into snow/ice, water, or bare-land for use in transportation applications and water management. Our test data set came from the UAVSAR Iceland deployment, covering fringe portions of Hofsjokull (glacier) on June 12<sup>th</sup>, 2009. Ground truth is scarce in this study; we obtained Landsat7 data from May 16<sup>th</sup>, 2009, however this is the beginning of the summer season and dramatic recession of snow cover can be seen. We limited our ground truth labels to conservative estimates of where the year-round glacial expanse occurs, limited areas of bare ground, and nearby lakes. Several hundred pixels from hundreds of thousands of labels were selected at random and provided as training labels along with the same feature set provided to the vegetation classifier. Approximately 50 support vectors were selected for the trained SVM.

Table 1 shows our classification accuracy as compared to the remaining labels. The results are promising, but this algorithm needs validation against additional data sets. We are presently processing newly collected data over the California Sierra Mountains, for which we have coincident Advanced Land Imager data for ground truth.

Table 1. Confusion matrix of snow/ice classifier against hand labels, data collected Jun 12th 2009.

	water	ice	land	count
no label	7%	10%	83%	16.7M
water	91%	3%	6%	145884
ice	3%	90%	7%	440706
land	1%	2%	96%	311201
<b>Total Accuracy: 829007 / 897791 (0.923385)</b>				

#### C. Disturbance Detection

Another rapid response application is to detect changes caused by natural hazards such as forest fires. A simple disturbance detection approach is to compare the amplitude images of two images acquired over the same target area, but separated in time. Each amplitude image is assigned a color channel in the composite image. Where there is no disturbance over time, the brightness, or gray scale features of the composite image indicate general backscatter magnitudes, and can allow interpretation of static features in the scene, such as topography and urban structures. Color changes indicate changes over time, and draw attention to disturbances. An example is shown in Figure 4, where data over the Angeles National Forest collected in February 2009 is composited with data collected in September 2009. Between these times the Station Fire burned some 160,000 acres of the forest, leaving a significant fire-scar, as can be seen in Figure 6. Blue areas in Figure 4 indicate where a stronger return was seen in February than in September, due to the loss of vegetation. Figure 5 uses the same data as in Figure 4, but highlights the areas of disturbance greater than 3 dB in magnitude, red for areas with a decrease in return over time and labeled as vegetated prior to

the fire, and green otherwise (more prominent in the urban area). Outlines of regions of non-disturbance in Figures 4 and 5 should be readily visible in the ASTER burn scar map in Figure 6, e.g. see the boot-like feature near the center top of the images.

#### IV. SUMMARY AND FUTURE WORK

Based on our prototype product analysis, surface water extent and disturbance detection show most reliable results, with the least computational costs. In the case of snow and ice classification, we need better ground truth to verify our results. We plan to implement the surface water extent algorithm on a platform similar to the RAD750, such as a single-board computer with PowerPC processors. This will provide better benchmarks for run-time requirements and allow for flight demonstration with UAVSAR. We also plan to investigate mudslide detection algorithms since we have many UAVSAR data sets of the San Gabriel Mountains to verify against local reports of mudslides as ground truth.

#### ACKNOWLEDGMENT

The work carried out in this paper was performed at Jet Propulsion Laboratory, California Institute of Technology under contract with the National Aeronautics and Space Administration (NASA). The authors wish to thank NASA's Earth Science Technology Office for funding this technology development through the Advanced Information System Technology program.

Copyright 2011 California Institute of Technology. Government Sponsorship acknowledged.

#### REFERENCES

- [1] Y. Lou, S. Chien, D. Clark, J. Doubleday, R. Muellerschoen, S. Saatchi, D. Tran, Y. Zheng, "A forest fire sensor web with UAVSAR," Proc. IGARSS Boston, 2008.
- [2] P. Dubois and J. van Zyl, "Measuring Soil Moisture with Imaging Radars," Trans. Geoscience and Remote Sensing, 1995.
- [3] B. Scheuchl, R. Caves, I. Cumming, and G. Staples, "Automated sea ice classification using spaceborne polarimetric SAR data," Proc. IGARSS Sydney, 3117-3119, 2001.



Fig. 4. Composite of repeat-pass HH backscatter images from Feb. 2009 (blue) and Sept. 2009 (red)

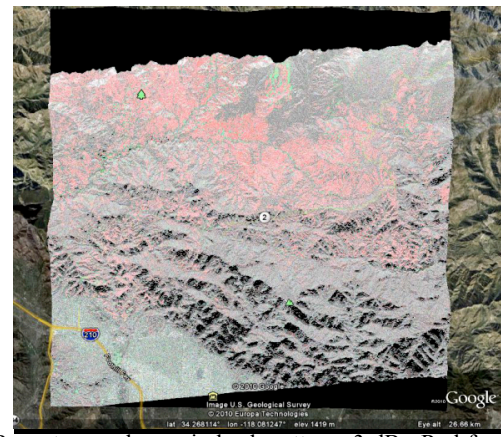


Fig. 5. Repeat pass change in backscatter > 3 dB. Red for vegetated areas (NLCD2001) and green for non-vegetated.

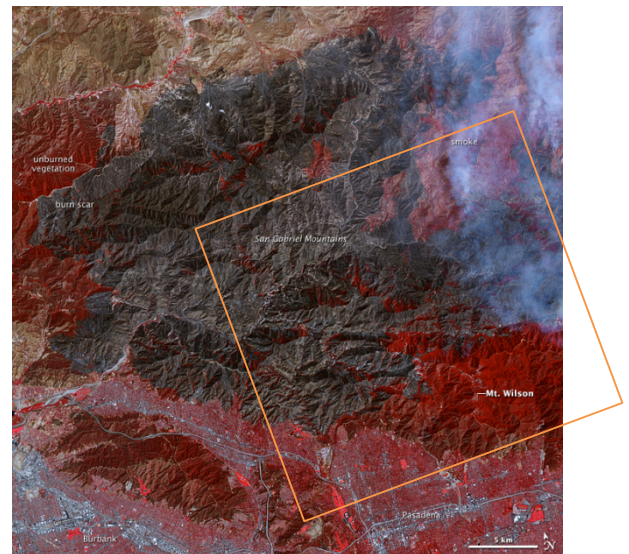


Fig. 6. ASTER image enhanced to contrast vegetation (red) and fire-scar (black/grey) (Allen 2009).